

The red supergiant and supernova rate problems: implications for core-collapse supernova physics

S. Horiuchi^{1,2,*}, K. Nakamura³, T. Takiwaki⁴, K. Kotake⁵, M. Tanaka⁶

¹*Center for Neutrino Physics, Department of Physics, Virginia Tech, Blacksburg, VA 24061, USA*

²*Center for Cosmology, Department of Physics and Astronomy, University of California, Irvine, CA 92697, USA*

³*Faculty of Science and Engineering, Waseda University, Ohkubo 3-4-1, Shinjuku, Tokyo 169-8555, Japan*

⁴*Center for Computational Astrophysics, National Astronomical Observatory of Japan, Mitaka, Tokyo 181-8588, Japan*

⁵*Department of Applied Physics, Fukuoka University, Fukuoka 814-0180, Japan*

⁶*National Astronomical Observatory of Japan, Mitaka, Tokyo 181-8588, Japan*

date

ABSTRACT

Mapping supernovae to their progenitors is fundamental to understanding the collapse of massive stars. We investigate the red supergiant problem, which concerns why red supergiants with masses $\sim 16\text{--}30M_{\odot}$ have not been identified as progenitors of Type IIP supernovae, and the supernova rate problem, which concerns why the observed cosmic supernova rate is smaller than the observed cosmic star formation rate. We find key physics to solving these in the compactness parameter, which characterizes the density structure of the progenitor. If massive stars with compactness above $\xi_{2.5} \sim 0.2$ fail to produce canonical supernovae, (i) stars in the mass range $16\text{--}30M_{\odot}$ populate an island of stars that have high $\xi_{2.5}$ and do not produce canonical supernovae, and (ii) the fraction of such stars is consistent with the missing fraction of supernovae relative to star formation. We support this scenario with a series of two- and three-dimensional radiation hydrodynamics core-collapse simulations. Using more than 300 progenitors covering initial masses $10.8\text{--}75M_{\odot}$ and three initial metallicities, we show that high compactness is conducive to failed explosions. We then argue that a critical compactness of ~ 0.2 as the divide between successful and failed explosions is consistent with state-of-the-art three-dimensional core-collapse simulations. Our study implies that numerical simulations of core collapse need not produce robust explosions in a significant fraction of compact massive star initial conditions.

Key words: stars: interiors – stars: massive – supernovae: general

1 INTRODUCTION

The association of core-collapse supernovae (SNe, including Types II and Ibc) with the death of massive stars is now firmly established both theoretically and observationally. Massive stars with initial mass between 10 and $30M_{\odot}$ evolve into red supergiants (RSG; e.g., Levesque et al., 2006) with extended envelopes that give rise to their spectral identification as hydrogen-rich Type II SNe upon core collapse. Higher mass stars that shed their outer envelopes evolve into naked helium or Wolf-Rayet stars (WR; Crowther, 2007) that eventually explode as hydrogen-free Type Ibc SNe. The transition from RSG to WR is expected to be a gradual one in mass, since metallicity, rotation, and binary mass transfer also significantly affect evolution. Nevertheless, observa-

tional estimates of the initial mass required to evolve into a WR is $\sim 30M_{\odot}$ (Massey et al., 2000), consistent with the maximum RSG mass. Theoretical studies also find the mass required for a single solar-metallicity star to shed its hydrogen envelope to be just above $25M_{\odot}$ (Heger et al., 2003; Eldridge & Tout, 2004). The link between RSGs and Type IIP SNe has been firmly established by advances in archival imaging of pre-SN progenitors (Smartt et al., 2009). Although similar strategies have not yet positively identified the progenitors of Type Ibc SNe, studies indicate the need for a significant contribution of binary stars to the Type Ibc SN progenitor population (Eldridge et al., 2013).

Advances have also revealed new puzzles. Smartt et al. (2009) identified what they termed the ‘‘RSG problem’’, which refers to the unknown fate of the most massive RSGs. Based on 20 Type IIP SNe with pre-images, the authors statistically derived an upper mass for Type IIP SN progenitors of $16.5^{+1.5}_{-1.5}M_{\odot}$ ($\sim 21M_{\odot}$ at 95% C.L.), which falls

* E-mail: horiuchi@vt.edu

short of the mass range of RSG populations that extend up to $\sim 30M_{\odot}$. Numerous explanations have been considered. For example, if the stellar initial mass function (IMF) is steeper, the null observation of massive RSG progenitors becomes statistically less significant (Smartt et al., 2009). Or, the loosely bound hydrogen envelopes of the most massive RSGs may become unstable and lost immediately prior to core collapse (e.g., Yoon & Cantiello, 2010). Pre-SN mass loss could also bias progenitor mass estimates to lower values due to insufficient dust correction (Walmswell & Eldridge 2012, but see Kochanek et al. 2012). Or, stellar evolution may limit the RSG mass to $\sim 20M_{\odot}$ (Groh et al., 2013). Finally, under certain conditions massive stars collapse to black holes (BH) with optically dark or faint “failed SNe” (e.g., Woosley & Heger, 2012; Lovegrove & Woosley, 2013), which may occur in the upper RSG mass range (Kochanek et al., 2008; Clausen et al., 2014; Kochanek, 2014a).

Another puzzle is the apparent dearth of observed cosmic SNe when compared to expectations from the cosmic star formation rate (SFR), termed the “SN rate problem” (Horiuchi et al., 2011). The mismatch is a factor of ~ 2 and consistently observed at all redshifts where cosmic SN rate data are available, except in the local $O(10)$ Mpc regime (Horiuchi et al., 2011; Botticella et al., 2012). Possible explanations involve a large fraction of optically dim SNe (Horiuchi et al., 2011), updates to the SFR calibrations (Horiuchi et al., 2013), and updates to dust corrections of SFR data (Mathews et al., 2014).

The picture is therefore more complex than a simplistic one where all massive stars evolve as single isolated stars and explode as luminous SNe. In this Letter, we investigate the success or failure of massive-star core collapse by focusing on the RSG and SN rate problems within a common theoretical framework using the “compactness” parameter, which quantifies the mass density structure of the SN progenitor. The importance of the compactness is well documented (e.g., Burrows & Lattimer, 1987; Fryer, 1999), especially in predicting the success or failure of core collapse (O’Connor & Ott, 2011; Ugliano et al., 2012). In particular, stars in the mass range $16\text{--}30M_{\odot}$ have large compactness, thus providing a solution to the RSG problem (Kochanek, 2014b). In this Letter, we show that the failed SN scenario naturally provides an explanation of the RSG and SN rate problems, and we use a series of two-dimensional numerical hydrodynamics simulations of core collapse, as well as state-of-the-art three-dimensional simulations, to support this scenario.

The Letter is organized as follows. In Section 2, we discuss the RSG and SN rate problems within a common framework of compactness. In Section 3, we discuss our hydrodynamics simulations and implications for the RSG and SN rate problems. We conclude with discussions in Section 4.

2 CHARACTERIZING THE PROBLEMS

The compactness encodes structural properties of the progenitor that critically affects whether the star will explode as a SN or not. It is defined as

$$\xi = \left. \frac{M/M_{\odot}}{R(M_{\text{bary}} = M)/1000 \text{ km}} \right|_t, \quad (1)$$

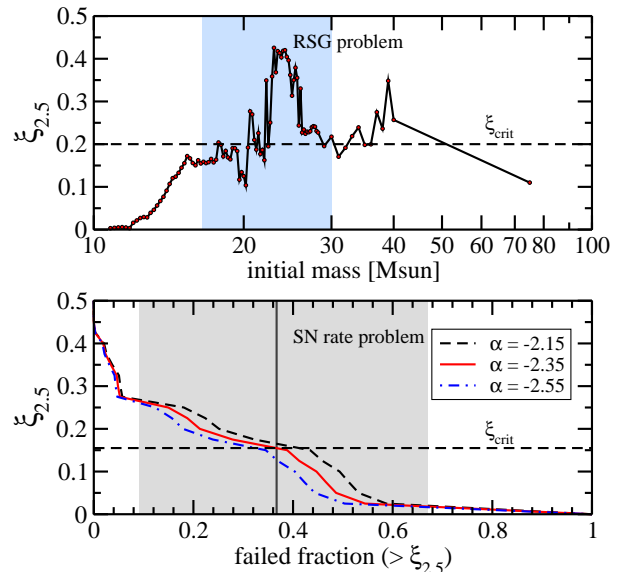


Figure 1. *Top:* the RSG problem, showing the compactness as a function of initial stellar mass, for the solar metallicity pre-SN progenitors of WHW02. The shaded band indicates the mass range of the RSG problem, and the horizontal dashed line guides the eye to the necessary critical compactness needed to solve the RSG problem. *Bottom:* the SN rate problem, showing the compactness as a function of the failed fraction, defined as the fraction of massive stars with a compactness above a critical $\xi_{2.5}$ value. Three IMFs are shown as labeled. The shaded band indicates the missing fraction inferred from data, and the dashed line guides the eye to the required critical compactness.

where $R(M_{\text{bary}} = M)$ is the radial coordinate that encloses a baryonic mass M at epoch t . The compactness is a measure of the shape of the mass density profile surrounding the iron core: the slower the density profile drop with radius, the larger the compactness. A shallower density gradient results in a larger accretion rate and hence ram pressure that a SN shock must overcome in order to turn what is initially an implosion into an explosion. Progenitors with higher compactness are therefore more difficult to explode (e.g., O’Connor & Ott, 2011; Ugliano et al., 2012; Nakamura et al., 2014b).

We adopt $M_{\text{bary}} = 2.5M_{\odot}$ at $t = 0$, i.e., the pre-SN epoch. While other definitions are possible, we find that $2.5M_{\odot}$ is sufficiently larger than the iron core mass but deep enough in the progenitor to affect the accretion rate during the critical moments of SN shock revival. As we demonstrate in Section 3, it shows a remarkable correlation with the qualitative result of the collapse, in particular in the vicinity of the parameter space for explosion failures. This is consistent with O’Connor & Ott (2011), where the compactness defined by $2.5M_{\odot}$ mass enclosed at time of bounce was used to distinguish between collapse to a neutron star (NS) or BH. Sukhbold & Woosley (2014) have shown how the compactness at the pre-SN epoch is just as useful as an indicator as the compactness derived at the time of core bounce. Therefore, we proceed to define the compactness at the pre-SN epoch and label this $\xi_{2.5}$.

The RSG problem in the language of compactness is illustrated in the top panel of Fig 1, where $\xi_{2.5}$ is shown as a function of the initial progenitor mass, for the solar metallic-

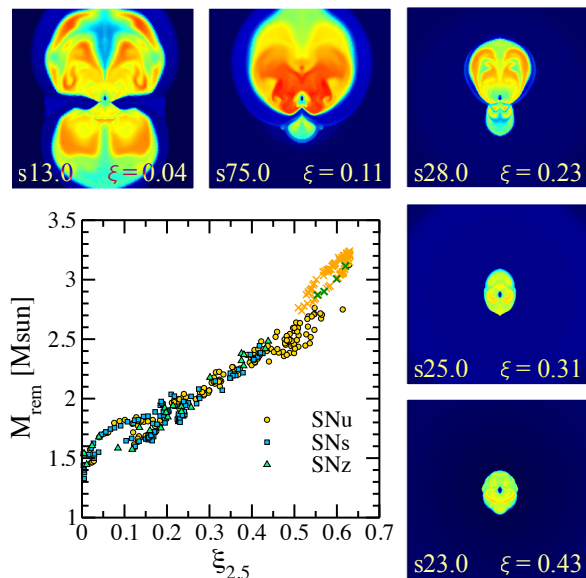


Figure 2. Remnant mass versus compactness. Each point corresponds to a two-dimensional simulation with a different progenitor. A clear trend of failed explosions (crosses) populating high $\xi_{2.5}$ is observed. The five panels show the entropy at 200 ms post bounce, from 5 to 25 k_B /baryon (blue–red). Each box is 2000 km on each side. Progenitors are chosen to cover a $\xi_{2.5}$ range 0.04–0.43.

ity models of Woosley et al. (2002) (WHW02). The value of $\xi_{2.5}$ depends non-monotonically on mass, and in particular, a peak exists between 20–30 M_{\odot} . The physics that determine the compactness is discussed in depth by Sukhbold & Woosley (2014), and involves the detailed burning history of the star. The peak is driven partly by smaller mass progenitors forming degenerate compact white dwarf-like cores that drive the compactness lower, but also by the disappearance of the first carbon shell burning in progenitors above $\sim 20M_{\odot}$ which increases the compactness since subsequent shell burnings are pulled down. While the exact features of $\xi_{2.5}$ are sensitive to the way semiconvection, convective overshooting, and mass loss are modelled, the qualitative peak features in mass are seen in multiple simulation codes (Sukhbold & Woosley, 2014). The shaded vertical column is the mass range of the RSG problem, i.e., 16.5–30 M_{\odot} (Smartt et al., 2009): these stars are missing from Type IIP SN progenitor searches. Therefore, massive stars with compactness above a critical value $\xi_{\text{crit}} \sim 0.2$ would need to not explode as canonically luminous Type IIP SNe.

The SN rate problem can be framed in terms of $\xi_{2.5}$ by estimating the fraction of all massive stars that have $\xi_{2.5}$ above some critical value. Physically, this fraction is interpreted as massive stars whose core density profile make it difficult to explode as canonical SNe, and is equivalent to an optically dim or dark SN fraction. Defining massive stars as 8–100 M_{\odot} stars, we derive this fraction for three IMFs $dN/dM \propto M^{\alpha}$ with $\alpha = -2.15, -2.35,$ and -2.55 , shown in the bottom panel of Fig 1. We quantify the SN rate problem using the latest data sets. The $z = 0$ SFR density is $0.015 \pm 0.003 h_{70} M_{\odot} \text{yr}^{-1} \text{Mpc}^{-3}$ and evolves as $(1+z)^{3.28}$ until $z \approx 1$ for the Salpeter-A IMF (Hopkins & Beacom, 2006, 2008). Adopting a mass range of 8–

100 M_{\odot} for stars producing SNe yields a SFR to SN rate conversion of $0.00965/M_{\odot}$ and hence a $z = 0$ SN rate density of $(1.5 \pm 0.25) \times 10^{-2} h_{70} \text{yr}^{-1} \text{Mpc}^{-3}$. We use a set of the most recent 13 SN rate measurements (Dahlen et al., 2004; Cappellaro et al., 2005; Botticella et al., 2008; Bazin et al., 2009; Li et al., 2011; Dahlen et al., 2012; Melinder et al., 2012; Taylor et al., 2014), and apply additional redshift-evolving dust correction as suggested in Mattila et al. (2012), except to Dahlen et al. (2012) and Melinder et al. (2012) that already implement such corrections. Adding statistical and systematic uncertainties in quadrature, and fitting a function $\dot{N}_0(1+z)^{\beta}$ to the data, we obtain $\dot{N}_0 = 0.92 \pm 0.15 \times 10^{-2} h_{70}^3 \text{yr}^{-1} \text{Mpc}^{-3}$ and $\beta = 3.4^{+0.6}_{-0.4}$. The missing SN fraction and its uncertainty, both derived from data, are shown by the vertical band. A critical compactness of ~ 0.15 therefore nominally solves the SN rate problem. Although the uncertainties are large, this is in the same range inferred to solve the RSG problem.

3 SIMULATIONS AND IMPLICATIONS

We use numerical simulations of SNe to provide interpretations of the critical compactness identified in the previous section. Our two-dimensional models (Nakamura et al., 2014b) are computed on a spherical polar grid of 384 radial zones from the center up to 5000 km and 128 angular zones covering $0 \leq \theta \leq \pi$, using the high-density EoS of Lattimer & Swesty (1991) with a nuclear incompressibility of $K = 220$ MeV. We employ the isotropic diffusion source approximation (Liebendörfer et al., 2009) and ray-by-ray approach to solve spectral transport of electron- and anti-electron neutrinos. Heavy-lepton neutrinos are treated by a leakage scheme to include cooling. We take into account explosive nucleosynthesis and its energy feedback into the hydrodynamics by solving a 13 α -nuclei network (Nakamura et al., 2014a). Our three-dimensional models use a grid of 64 angular zones and 128 azimuthal zones (Takiwaki et al., in preparation).

The two-dimensional simulations are performed on the full set of solar- (s), 10^{-4} solar (u), and zero-metallicity (z) progenitors of WHW02, a total of 377 progenitor initial conditions. This allows systematic trends to be explored. Fig 2 shows one such trend, showing the remnant mass, defined as the mass within a density coordinate of 10^{11}gcc^{-1} , as a function of the progenitor $\xi_{2.5}$, for all the s-, u- and z- models. Simulations that fail to reach a successful explosion, as defined by the shock radius not reaching a radius of 400 km within the first 1.5 s of simulation time (equivalent to ~ 1.2 s in time since bounce), are marked by crosses. These failed explosions clearly populate the highest $\xi_{2.5}$ and confirm the predictive power of using $\xi_{2.5}$ to distinguish the outcome of core collapse. In fact, the compactness is a continuous measure of explosibility: the small panels of Fig 2 show how the explosion becomes increasingly smaller with higher $\xi_{2.5}$.

Fig 2 implies that the division between successful (filled points) and failed (crosses) explosions is $\xi_{2.5} \sim 0.5$, i.e., a critical compactness that is significantly larger than the observationally inferred critical value of $\xi_{\text{crit}} \sim 0.15$ –0.2. However, there are issues that complicate such a conclusion. First, many of the successful explosions with large compactness will likely not explode as canonical SNe. For our EOS, the maximum NS mass is $\sim 2.4M_{\odot}$ (e.g., Müller et al.,

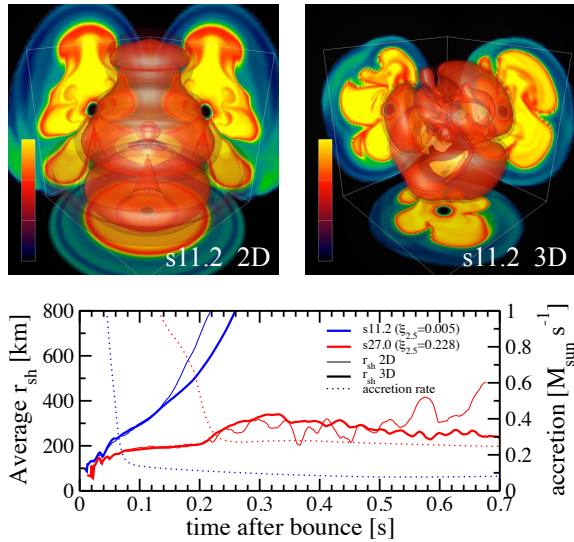


Figure 3. *Top:* snapshots of the entropy distribution of s11.2 at 200 ms post bounce in 2D (left) and 3D (right), illustrating the smaller nature of 3D explosions. Each cube is 1000 km on each side, and the colour covers 5–16 k_B /baryon (black–yellow). *Bottom:* average shock radius r_{sh} (solid line, left axis) for 2D (thin line) and 3D (thick line) simulations, and the mass accretion rate \dot{M} (dotted line, right axis), all for two progenitors: s11.2 (blue) and s27.0 (red). 2D simulations experience earlier shock revival, and higher $\xi_{2.5}$ corresponds to later shock revival.

2012), so the remnants of progenitors with $\xi_{2.5} \gtrsim 0.4$ would collapse to BHs. Thus, these SNe will be dimmer due to mass fall back. Second, additional physics are considered to be important in accurately predicting the outcome of core collapse, including general relativity and weak interaction physics (see recent reviews, Kotake et al., 2012; Janka et al., 2012). Also, studies suggest that stars explode more easily in two dimensions than in three (e.g., Hanke et al. 2012; Pejcha & Thompson 2012; Couch 2013; Takiwaki et al. 2014). All of these can shift the location of the critical compactness for a successful explosion.

In order to provide a more realistic interpretation, we run select progenitors in both 2D and 3D. The lower panel of Fig 3 shows the average shock radius (left y-axis) for 2D (solid) and 3D (thick solid), and the mass accretion rate (dashed, right y-axis), for the s11.2 M_{\odot} and s27.0 M_{\odot} progenitor models of WHW02. The importance of $\xi_{2.5}$ is once again observable: while s11.2 M_{\odot} ($\xi_{2.5} = 0.005$) comfortably explodes, s27.0 M_{\odot} ($\xi_{2.5} = 0.228$) does not (Takiwaki et al., 2014). A more subtle but important point is that SN shock revival is slower in 3D than in 2D. This is clearly the case for s11.2 M_{\odot} , where the 3D shock radius grows slower than the 2D shock radius. For s27.0 M_{\odot} , the 3D shock radius shows no signs of revival, while the 2D shock does. These results are consistent with those of Hanke et al. (2013). The upper panels of Fig 3 show the entropy distribution for the s11.2 M_{\odot} progenitor in 2D (left) and 3D (right), both at 200 ms post-bounce, illustrating how explosions are larger in 2D compared to the more round and compact 3D case.

Fig 4 illustrates the impact of dimensionality on the critical compactness. The solid curve shows the fraction of progenitors that successfully explode in our 2D simulations

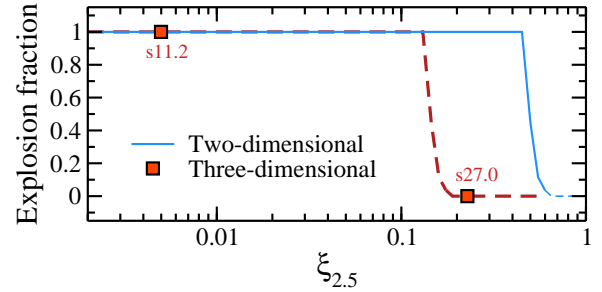


Figure 4. The fraction of successful SN explosions as functions of the compactness $\xi_{2.5}$. Shown are the results from 377 2D simulations (in solid) and results from two 3D simulations (square symbols). The dashed curve connects the 3D results whilst keeping the same shape as the 2D results.

binned in $\xi_{2.5}$. The plateau and sharp decline in the explosion fraction illustrates the power of using $\xi_{2.5}$ as an indicator of the core collapse outcome. The square symbols show the results of 3D simulations. Each square corresponds to an individual progenitor as labeled. Interestingly, they support a quantitatively different picture, with the critical compactness being $\xi_{2.5} \sim 0.2$ or less. Only a limit can be stated due to the small number of progenitors simulated in 3D. Nevertheless, 3D simulations at present indicate it is possible for the critical compactness to be close to that required from observations.

4 DISCUSSIONS AND CONCLUSIONS

We have argued that current stellar and core-collapse simulations are consistent with the RSG and SN rate problems if all stars with compactness above a critical value of $\xi_{\text{crit}} \sim 0.2$ collapse to form BHs and do not successfully produce canonically luminous SNe, i.e., failed SNe. We explicitly demonstrate how the compactness of the progenitor strongly impacts the outcomes of core collapse (Fig 2), and that the required critical compactness (Fig 1) is compatible with state-of-the-art simulations (Fig 4).

There are several observational consequences of this scenario. In fact, similar values of ξ_{crit} have been previously inferred by consideration of remnant mass functions. Kochanek (2014a,b) show how the failed SN scenario reproduces the observed NS and BH mass functions without fine-tuning stellar evolution or core-collapse physics.

Secondly, the implied failed SN fraction is $f_{\text{BH}} \sim 20\text{--}40\%$, including stars in the 16.5–30 M_{\odot} range and additional contribution from stars around $\sim 40M_{\odot}$. The value of f_{BH} is presently only weakly constrained by data, but this is poised to improve. The diffuse SN neutrino background currently limits $f_{\text{BH}} \lesssim 50\%$ (Lien et al., 2010), but will improve with more data taking (Horiuchi et al., 2009; Yuksel & Kistler, 2012). Campaigns searching for disappearance of massive stars will obtain 90% bounds down to $f_{\text{BH}} \sim 20\text{--}30\%$ in 10 years observing (Kochanek et al., 2008). Galactic data also provide some probe (Adams et al., 2013).

Thirdly, the scenario has implications for SN types and their progenitors. Consider a simple model where (i) 8–16.5 M_{\odot} stars produce IIP SNe, unless modified by binary interactions in which case they produce Ibc or Iib SNe, (ii)

16.5–30 M_{\odot} stars produce failed SNe, and (iii) 30–40 M_{\odot} stars produce Ibc or IIb SNe. We ignore the other Type II (IIa, IIc, etc) SNe here as they are a minority (Li et al., 2011) and we assume them to be distributed across the full range of stellar masses (Smith et al., 2011). The IIP/(Ibc+IIb) ratio is then $0.015(1 - f_b)/(0.015f_b + 0.0013)$, where f_b is the binary fraction. The observed IIP/(Ibc+IIb) ratio ≈ 2.1 (Li et al., 2011) is then reproduced for a binary fraction $f_b \sim 0.3$, which is within current estimates based on O star statistics (e.g., Sana et al., 2012). This scenario predicts that 3/4 of Ibc SNe arise from binary stripped stars of initial mass $< 16.5M_{\odot}$.

The main limitation of our study is the inherent uncertainties in the progenitor models that we have explored. The 1D progenitor models of WHW02 have the advantage of being the largest set of models currently available, but there are important uncertainties that must be highlighted. The treatment of turbulent transport and mixing inside the star is a source of significant uncertainty, and studies have begun to reveal just how important realistic treatments beyond the mixing-length style treatments are (e.g., Meakin et al., 2011; Smith & Arnett, 2014). Notably, the 1D progenitor models of Limongi & Chieffi (2006) do not show a peak in $\xi_{2.5}$ around $\sim 20M_{\odot}$ seen in WHW02, although the number of progenitors is limited. On the other hand, Sukhbold & Woosley (2014) observe the peaks with the MESA code. Further works are therefore required to reveal whether the peak is a robust feature of stellar evolution or not.

More data and studies will also help reveal the severity of the RSG and SN rate problems and hence importance of our scenario. For example, dynamical modelling of SNe can help increase the number of SNe with progenitor mass estimates. At present, however, such mass estimates vary widely for any given SNe, highlighting the large systematic uncertainties involved. The significance of the SN rate problem will also be tested by future SFR data, and also as the systematics of SFR dust correction are studied further.

In summary, modern studies of SN progenitors collectively point to a non-negligible fraction of massive stars potentially failing to produce successful SNe. We have explored a connection of such observational features to the physics of core-collapse, namely, the compactness of the progenitors. We demonstrate how modern simulations support a trend of failed explosions at precisely where observations indicate potential failed explosions. An intriguing implication, then, is that the failures of many supernova simulations in producing robust explosions may actually be closer to reality than previously thought.

Acknowledgments

We thank John Beacom and Chris Kochanek for discussions and comments. SH is supported by a Research Fellowship for Research Abroad by JSPS. This study was supported in part by the Grants-in-Aid for the Scientific Research from the Ministry of Education, Science and Culture of Japan (Nos. 26870823, 24244036, 24103006, 26707013, 24740117, and 25103515) and by HPCI Strategic Program of Japanese MEXT, and used computational resources of the K

computer at AICS through the HPCI project (ID:hp120304) and XC30 at NAOJ.

References

- Adams, S. M., et al. 2013, ApJ, 778, 164
 Bazin, G., et al. 2009, A&A, 499, 653
 Botticella, M. T., et al. 2008, A&A, 479, 49
 Botticella, M. T., et al. 2012, A&A, 537, A132
 Burrows, A., & Lattimer, J. M. 1987, ApJ, 318, L63
 Cappellaro, E., et al. 2005, A&A, 430, 83
 Clausen, D., et al. 2014, arXiv:1406.4869
 Couch, S. M. 2013, ApJ, 775, 35
 Crowther, P. A. 2007, ARA&A, 45, 177
 Dahlen, T., et al. 2004, ApJ, 613, 189
 Dahlen, T., et al. 2012, ApJ, 757, 70
 Eldridge, J. J., et al. 2013, MNRAS, 436, 774
 Eldridge, J. J., & Tout, C. A. 2004, MNRAS, 353, 87
 Fryer, C. L. 1999, ApJ, 522, 413
 Groh, J. H., et al. 2013, A&A, 558, A131
 Hanke, F., et al. 2012, ApJ, 755, 138
 Hanke, F., et al. 2013, ApJ, 770, 66
 Heger, A., et al. 2003, ApJ, 591, 288
 Hopkins, A. M., & Beacom, J. F. 2006, ApJ, 651, 142
 Hopkins, A. M., & Beacom, J. F. 2008, ApJ, 682, 1486
 Horiuchi, S., et al. 2009, Phys. Rev. D, 79, 083013
 Horiuchi, S., et al. 2011, ApJ, 738, 154
 Horiuchi, S., et al. 2013, ApJ, 769, 113
 Janka, H.-T., et al. 2012, PTEP, 2012, 010000
 Kochanek, C. S., et al. 2008, ApJ, 684, 1336
 Kochanek, C. S., Khan, R., & Dai, X. 2012, ApJ, 759, 20
 Kochanek, C. S. 2014, ApJ, 785, 28
 Kochanek, C. S. 2014, arXiv:1407.5622
 Kotake, K., et al. 2012, PTEP, 2012, 010000
 Lattimer J., & Swesty D. 1991, Nucl. Phys. A, 535, 331
 Levesque, E. M., et al. 2006, ApJ, 645, 1102
 Li, W., et al. 2011, MNRAS, 412, 1473
 Liebendörfer, M., et al. 2009, ApJ, 698, 1174
 Lien, A., et al. 2010, Phys. Rev. D, 81, 083001
 Limongi, M., & Chieffi, A. 2006, ApJ, 647, 483
 Lovegrove, E., & Woosley, S. E. 2013, ApJ, 769, 109
 Massey, P., et al. 2000, AJ, 119, 2214
 Mathews, G. J., et al. 2014, ApJ, 790, 115
 Mattila, S., et al. 2012, ApJ, 756, 111
 Meakin, C. A., et al. 2011, Ap&SS, 336, 123
 Melinder, J., et al. 2012, A&A, 545, A96
 Müller, B., Janka, H.-T., & Marek, A. 2012, ApJ, 756, 84
 Nakamura, K., et al. 2014, ApJ, 782, 91
 Nakamura, K., et al. 2014, arXiv:1406.2415
 O’Connor, E., & Ott, C. D. 2011, ApJ, 730, 70
 Pejcha, O., & Thompson, T. A. 2012, ApJ, 746, 106
 Sana, H., et al. 2012, Science, 337, 444
 Smartt, S. J., et al. 2009, MNRAS, 395, 1409
 Smith, N., & Arnett, W. D. 2014, ApJ, 785, 82
 Smith, N., et al. 2011, MNRAS, 412, 1522
 Sukhbold, T., & Woosley, S. E. 2014, ApJ, 783, 10
 Takiwaki, T., Kotake, K., & Suwa, Y. 2014, ApJ, 786, 83
 Taylor, M., et al. 2014, arXiv:1407.0999
 Ugliano, M., et al. 2012, ApJ, 757, 69
 Walmswell, J. J., & Eldridge, J. J. 2012, MNRAS, 419, 2054

- Woosley, S. E., et al. 2002, *Rev. Mod. Phys.*, 74, 1015
Woosley, S. E., & Heger, A. 2012, *ApJ*, 752, 32
Yoon, S.-C., & Cantiello, M. 2010, *ApJ*, 717, L62
Yuksel, H., & Kistler, M. D. 2012, *arXiv:1212.4844*